Design and Performance of a Horizontal Mooring for Upper-Ocean Research

MARK GROSENBAUGH

Department of Applied Ocean Physics and Engineering, Woods Hole Oceanographic Institution, Woods Hole, Massachusetts

STEVEN ANDERSON AND RICHARD TRASK

Department of Physical Oceanography, Woods Hole Oceanographic Institution, Woods Hole, Massachusetts

JASON GOBAT AND WALTER PAUL

Department of Applied Ocean Physics and Engineering, Woods Hole Oceanographic Institution, Woods Hole, Massachusetts

BRADFORD BUTMAN

U.S. Geological Survey, Woods Hole Field Center, Woods Hole, Massachusetts

ROBERT WELLER

Department of Physical Oceanography, Woods Hole Oceanographic Institution, Woods Hole, Massachusetts

(Manuscript received 25 May 2001, in final form 16 January 2002)

ABSTRACT

This paper describes the design and performance of a two-dimensional moored array for sampling horizontal variability in the upper ocean. The mooring was deployed in Massachusetts Bay in a water depth of 84 m for the purpose of measuring the horizontal structure of internal waves. The mooring was instrumented with three acoustic current meters (ACMs) spaced along a 170-m horizontal cable that was stretched between two subsurface buoys 20 m below the sea surface. Five 25-m-long vertical instrument strings were suspended from the horizontal cable. A bottom-mounted acoustic Doppler current profiler (ADCP) was deployed nearby to measure the current velocity throughout the water column. Pressure sensors mounted on the subsurface buoys and the vertical instrument strings were used to measure the vertical displacements of the array in response to the currents. Measurements from the ACMs and the ADCP were used to construct time-dependent, two-dimensional current fields. The current fields were used as input to a numerical model that calculated the deformation of the array with respect to the nominal zero-current configuration. Comparison of the calculated vertical offsets of the downstream subsurface buoy and downstream vertical instrument string with the pressure measurements were used to verify the numerical code. These results were then used to estimate total deformation of the array due to the passage of the internal waves. Based on the analysis of the three internal wave events with the highest measured vertical offsets, it is concluded that the geometry of the main structure (horizontal cable and anchor legs) was kept to within ± 2.0 m, and the geometry of the vertical instrument strings was kept to within ± 4.0 m except for one instance when the current velocity reached 0.88 m s^{-1}.

1. Introduction

The ability of oceanographers to fully visualize, measure, and understand physical processes in the upper ocean is hampered by our inability to deploy arrays of closely spaced instruments in horizontal directions. The single-point moorings that are typically used in oceanography (Berteaux 1991) allow the deployment of sensors (e.g., temperature, salinity, sound speed, bio-optical properties, and current speeds) with vertical spacing of less than 1 m. Such moorings can be deployed in arrays (Weller et al. 1990); however, the anchors are usually separated by distances at least equal to the water depth in order to prevent tangling of the mooring lines. In deep water, this restricts the horizontal separation of the sensors on neighboring moorings to scales on the order of kilometers. Being able to deploy arrays of instruments with much smaller horizontal separations is essential to increasing our knowledge of the spatial variability in the upper ocean and its temporal evolution.

The goal of the development effort reported in this paper was to design, build, deploy, and recover a pro-

Corresponding author address: Mark A. Grosenbaugh, Woods Hole Oceanographic Institution, Mail Stop 7, Woods Hole, MA 02543.
E-mail: mgrosenbaugh@whoi.edu

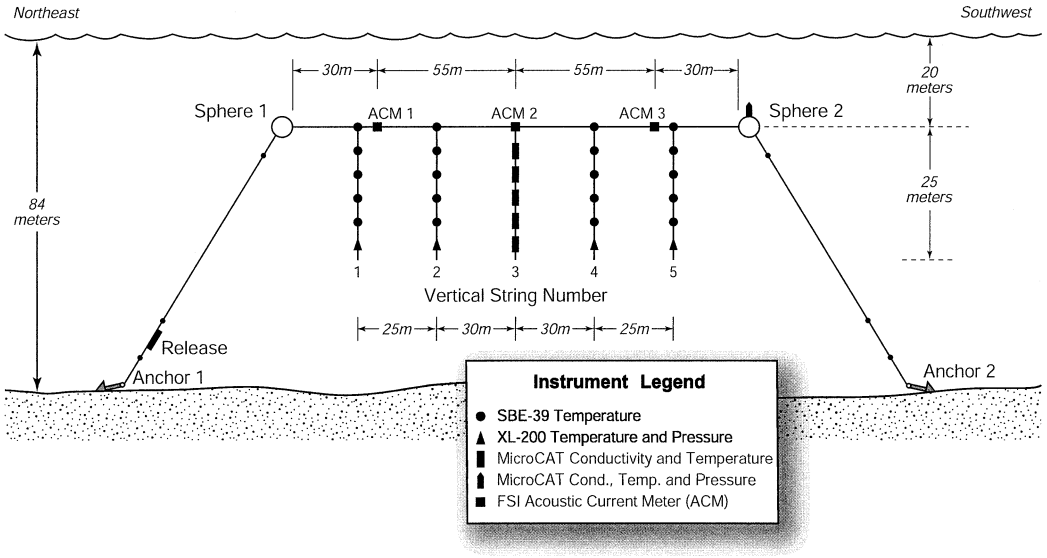

FIG. 1. Engineering drawing of the horizontal mooring.

totype two-dimensional cable system (Fig. 1) that had instruments distributed both horizontally and vertically in the near-surface layer of the ocean. The mooring was designed for deployment along coastal margins in depths up to 200 m. Such an effort would demonstrate the feasibility of using such moorings for oceanographic measurements in coastal environments, paving the way for deploying multiple horizontal arrays to investigate three-dimensional variability on scales of meters to hundreds of meters.

The deployment of horizontal cables in the ocean is not new. The Navy Civil Engineering Laboratory deployed a cable structure that consisted of three subsurface moorings connected at the buoys by three horizontal cables forming a horizontal delta-shaped array (Kretshmer et al. 1975). The mooring was deployed in nearly 900 m of water in the Santa Monica Basin off California. The horizontal cables were 300 m long and were moored approximately 150 m below the sea surface. The purpose of the mooring was to collect engineering data on the steady-state response of a complex cable structure to ocean currents and to compare the measurements with numerical methods for predicting static mooring configurations (Skop et al. 1977). The mooring was instrumented with six acoustic transponders and six pressure sensors to measure cable position and five tension cells to measure mooring-line loads. Recording equipment housed in a separately moored subsurface buoy, which was connected to the delta mooring by electromagnetic cables, collected the data from these sensors. Separate subsurface moorings were used to measure current velocities.

Berteaux and Walden (1981) proposed a number of design variations for deep-sea cable arrays that included novel configurations that stiffened the structures against currents. They used the numerical methods developed by Skop and Mark (1973) to perform calculations of the static forces and displacements due to uniform currents. They concluded that it was feasible to build and deploy structures with horizontal elements stretching over kilometers in the deep ocean, though none was ever deployed.

More recently, the aquaculture industry has developed horizontal arrays as platforms to grow shellfish. These structures are deployed in rows of submerged ''long-line'' moorings (Bonardelli 1996; Goudey and Smolovitz 1996; Thomson 1996) with either seed grow-out ropes or rows of lantern grow-out nets suspended vertically from a horizontal rope. They were developed mostly from the experience of fisherman rather than engineering studies. These systems, deployed in coastal waters and sheltered bays, have horizontal cables that span up to 300 m and are placed near the surface to facilitate access to the shellfish crop. Until recently, the aquaculture arrays have been deployed in sheltered areas to avoid the effects of ocean waves. People are now considering the deployment of these systems in the open ocean.

The horizontal array discussed in this paper represents the next step in the development and deployment of these types of systems for oceanographic applications. With regards to measuring upper-ocean variability, there are much more stringent demands placed on the ability of the array to maintain its shape in response to environmental forcing. An important result of this paper is the analysis of the position errors (i.e., the offsets from the nominal zero-current configuration) of the sensors due to currents and waves. Our initial analysis will show, in general, under what types of conditions the horizontal array can be used successfully. We will then present data from an actual deployment in which the array was used to measure horizontal and vertical var-

iability in an internal wave field. Using current measurements and pressure data we show that the mooring was able to maintain its geometric configuration within specifications for nearly all of the observed internal wave events. We also use this opportunity to verify numerical tools, which can be used in the future to design similarly shaped oceanographic cable arrays and aquaculture moorings.

2. The horizontal mooring

The starting point for our design was based on aquaculture long-line moorings but with vertical strings of oceanographic sensors replacing the grow-out ropes and nets. We then applied numerical modeling techniques to examine the static and dynamic characteristics of the mooring in terms of performance and survivability, making design changes where needed to meet the specifications that are detailed below.

During the course of this study, two separate horizontal moorings were built and deployed (Trask et al. 1999). The first mooring was deployed in the summer of 1997 near Provincetown, Massachusetts. It was used to test the anchors and work out the deployment schemes, among other things. A second array was deployed in the summer of 1998 in Massachusetts Bay with a goal of verifying numerical simulations and demonstrating the platform's capability for gathering scientific data (Anderson et al. 1999). This paper discusses the design and performance of the second array.

The horizontal array (Fig. 1) was constructed using a pair of vertical subsurface moorings with a horizontal cable suspended in between. Each subsurface mooring consisted of a 48-in. steel sphere, a length of 3/8-in. jacketed wire rope, a length of ½-in. trawler chain, a length of 1¼ in. steamer chain, and an anchor. One of the subsurface mooring legs was fitted with an in-line acoustic release. Adjustments in the lengths of the two subsurface mooring legs were made to account for a difference in the net buoyancy of the spheres. The left-hand sphere in Fig. 1 had net buoyancy of 6586 N compared to net buoyancy of 5207 N for the right-hand sphere.

Stretched between the two subsurface spheres at a nominal depth of 20 m was a 170-m horizontal cable consisting of four pieces of 3/8-in. wire rope swaged at the ends. Three Falmouth Scientific, Inc. acoustic current meters (model 3D-ACM) were deployed in-line with the horizontal wire at the swage fittings. The positions of the current meters were 30, 85, and 140 m measured from one end of the horizontal cable. Five 25-m long vertical instrument strings were attached to the horizontal cable at positions of 25, 55, 85, 115, and 145 m from the end. One vertical instrument string was hung from the central current meter, and the other four strings were clamped to the horizontal wire using PVC plates. The vertical strings were made from 3/16-in. jacketed wire rope. The central instrument string that hung below the middle current meter consisted of five SeaBird Electronics MicroCAT SBE-37-IM temperature and conductivity sensors spaced 5 m apart starting 5 m below the current meter. The bottom MicroCAT also contained a pressure sensor (0–100-m range). The other vertical instrument strings consisted of five SeaBird Electronics SBE-39 temperature-recording instruments (spaced 5 m apart starting 5 m below the horizontal cable) and one Brancker Research, Ltd. XL-200 temperature and pressure instrument (attached 5 m below the bottom SBE-39 temperature sensor). Sash weights weighing up to 350 N (in air) were attached to the bottom of the instrument strings to minimize horizontal offsets due to currents. A pair of 17-in. glass balls (total buoyancy of 498 N per pair) was attached above each vertical instrument string. In addition a pair of plastic floats (total buoyancy of 39 N per pair) was attached above the two off-centered current meters. The buoyancy was used to offset the weight of the instruments and prevent the horizontal cable from sagging. Separate MicroCAT temperature, conductivity, and pressure sensors were placed on the subsurface buoys, though the system on sphere 1 failed to work properly. Sphere 2 had a 6 degree-of-freedom motion-recording package mounted inside. A SeaBird Electronics tide gauge was mounted on the anchor of a nearby subsurface mooring to give reference pressure. Additional graphical details of the horizontal array are given in Trask et al. (1999).

Specifications were chosen for the expected mooring performance during operations (design specifications) and during severe storms (survival specifications). The design specifications called for the mean positions of the instruments to be within ± 2.0 m of their nominal positions (i.e., positions with zero current present). This specification proved to be too ambitious with regards to the vertical instrument strings, and it was modified to allow for ± 4.0 m of mean offset of the bottom of the strings. The dynamic motion (about the mean positions) of the instruments was specified to have maximum amplitude of less than 0.5 m. Design conditions were assumed to be a uniform current of 0.5 m s^{-1} and Sea State 4 (significant wave height of 2.6 m and peak period of 8.4 s). The specification of 0.5 m s^{-1} uniform current again proved to be slightly ambitious. Alternatively, we analyzed the mooring under different uniform current speeds and directions and determined the maximum operating conditions under which the design specifications were met. We repeated this procedure with an idealized unidirectional current field for an internal wave with magnitudes that varied sinusoidally in the horizontal direction and decreased linearly in the vertical direction.

The survival specifications required that the mooring not drift and the components not fail in strong currents and large storms. A uniform current of 1.0 m s^{-1} was chosen for the survival current profile, which was above the maximum currents that had been measured previously for the region (Geyer et al. 1992). The survival sea state

was chosen as Sea State 8 (significant wave height 7.5 m, 12.5-s period). This is the largest sea state that was observed in Massachusetts Bay from 1993 to 1997 and occurred during a storm in April 1997 as documented by the National Data Buoy Center's moored buoy station that is just east of Boston, Massachusetts (see historical data records of moored station 44013 for years 1993–97 online at www.ndbc.noaa.gov). Though the 1998 deployment was to take place during August 1998 and last for approximately 30 days, we chose wave conditions as if the deployment was for a period of 1 yr.

The results of the survival analysis, as presented in the next section, were used to properly size the mooring components to withstand the expected maximum loads. After this, the most important factor for the survivability of the horizontal array was the anchor holding force. In initial designs, the mooring geometry required that the anchors hold a tension that was directed between 30° and 45° from the horizontal. In 1997, we conducted several field tests at these angles to determine the holding capability of three types of cast-iron anchors—a cylindrical dome-shaped anchor, a modified cylindrical anchor with steel plates protruding from the bottom, and a pyramid anchor developed by DorMor, Inc. (Trask et al. 1999). The tests were conducted on sandy and muddy bottoms in Vineyard Sound, Massachusetts. The DorMor anchor had the best performance characteristics for this application, having a sliding force of between 1.0 and 1.1 times its own weight in water while being pulled over the bottom. The peak force (i.e., the force needed to break the anchor free and start it moving) was between 1.5 and 2.1 times its weight in water. Additional tests with the same experimental setup were performed in 1998 with the DorMor anchor at a site with a soft muddy bottom. Here, the anchor dragged smoothly at a constant tension equal to its weight in water. In the final design, a 2000-lb DorMor anchor and a 1000-lb DorMor anchor (placed in series as backup) were used to fix the ends of the mooring. The 1¼-in. steamer chain that was placed just above the 2000-lb anchors helped lower the mooring-line angle, which increased the holding force of the anchors according to the manufacturer's specifications. The deployment procedure for the anchors and other components of the horizontal array is described in Trask et al. (1999).

3. Engineering analysis

We will first describe the results of applying the survival conditions of velocity of 1.0 m s^{-1} and Sea State 8 to determine maximum loads on the different components including the anchors. We will then describe how these values were used to finalize the overall mooring configuration in terms of the depths of the subsurface buoys, the lengths and angles of the mooring lines, the tensions in the mooring lines and horizontal cable, and the loads on the anchor. This will be followed by the design analysis using uniform currents and spatially varying currents to determine operating performance. The final piece of the analysis (to be presented in the next section) will be to determine the instrument response during the actual deployment due to the passage of internal waves.

The engineering calculations were performed using a general-purpose numerical code, developed at Woods Hole Oceanographic Institution (WHOI), for calculating statics and dynamics of moored and towed oceanographic systems (Gobat and Grosenbaugh 2000). The finite-difference time domain simulation is built around a mathematical model of cable dynamics that includes the effects of geometric and material nonlinearities, bending stiffness, and torsion. This permits accurate three-dimensional dynamic modeling of systems even in cases when the cable goes slack. The nonlinear, one-sided boundary condition at the seabed is modeled as an elastic foundation that supports the cable when it is lying on the bottom. The numerical implementation includes an adaptive time stepping algorithm and adjustable numerical dissipation (Gobat and Grosenbaugh 2001) to facilitate the solution of problems with strong nonlinearities. For this particular application, we developed new features for handling multileg moorings and suspended cables with hanging masses. The static and dynamic algorithms used in the numerical simulations have been verified extensively for single-point, deep-water and single-point, shallow-water moorings (Gobat and Grosenbaugh 1998). Comparisons in the next section between simulations and measurements are used to verify the numerical model of the moored horizontal array.

The most critical parameters of the numerical model, in this case, were the drag coefficients of the subsurface buoys and the wire rope. Comparison with data, presented in the next section, showed a good match with drag coefficients of 0.5 for the spherical subsurface buoys and 2.0 for the wire rope. These values are slightly higher than reported values, measured in the laboratory for fixed smooth spheres and fixed smooth circular cylinders (Hoerner 1965), but are representative of objects that are vibrating in response to flow (Blevins 1990). In particular, Williamson and Govardhan (1997) measured a drag coefficient of between 0.4 and 0.8 for a tethered sphere vibrating with amplitude of up to 0.5 diameters and at Reynolds numbers up to 14 000. Even though our Reynolds numbers are much higher (up 8 $\times$ 10^5), a drag coefficient of 0.5 appears reasonable based on measured vibration amplitudes of up to 0.2 diameters. Very low drag coefficients (i.e., $C_d \approx 0.2$) that are observed in the laboratory for Reynolds numbers greater than about 3×10^5 would probably not be seen in this case because the spheres are rough with a number of attached appendages and the ambient current is highly turbulent.

The final configuration (Fig. 1) of the mooring had a 170-m-long horizontal cable and mooring legs that were approximately 87 m (left mooring leg) and 96 m

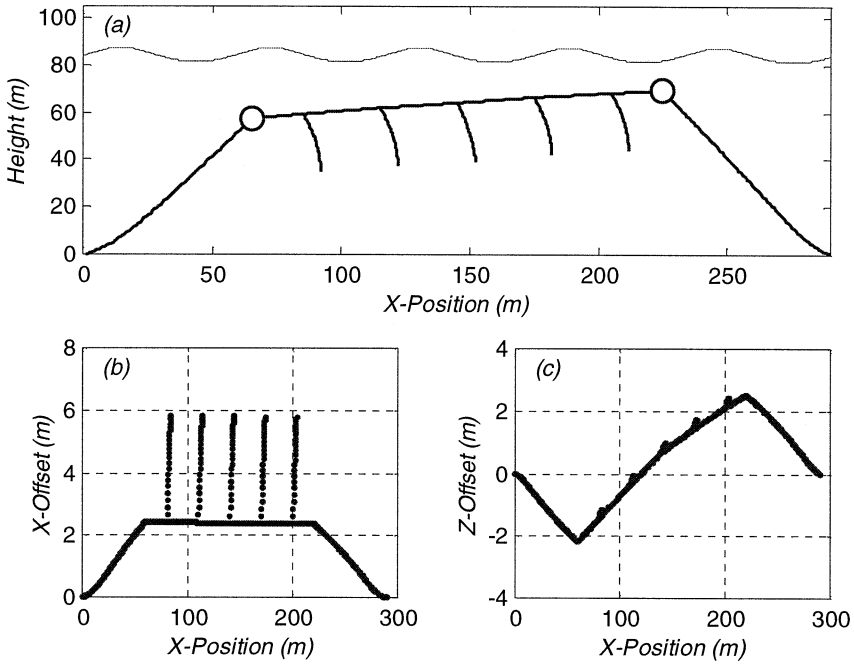

FIG. 2. Calculated static shape and offsets of the mooring in a 0.5 m s^{-1} uniform current that is parallel to the array plane. (a) The deformation of the array, which occurs in a two-dimensional plane. (b) The horizontal offsets. (c) The vertical offsets of the anchor legs, horizontal cable, and vertical instrument strings as a function of the nominal horizontal position.

(right mooring leg) in length due to the difference in buoyancy of the subsurface spheres. The spread of the mooring (i.e., the horizontal distance between the anchors) was 290 m. The final configuration was a tradeoff between minimizing the spread of the mooring, maximizing the stiffness of the mooring with respect to currents, and limiting the anchor size. The latter specification was dictated by the capabilities of the ship that was used to deploy the array. By increasing the mooring-line length and lowering its angle at the buoy, we were able to increase the tension in the horizontal cable. This stiffened the mooring against currents, but it increased the spread and the size of the anchors that were needed. In the final analysis, the holding ability of the 2000-lb DorMor anchor (weight in water of 8510 N) in survival conditions dictated the geometry of the array.

a. Survival conditions

The maximum static anchor load calculated using the survival current of 1 m s^{-1} was 7830 N. This load occurred on the left-hand anchor (Fig. 1) when the current was oriented parallel to the horizontal cable and flowing from left to right. Reversing the current produced a static pull on the right-hand anchor of 7630 N. The asymmetry was due to the difference in the buoyancy of the subsurface spheres and the lengths of the vertical mooring lines, as previously noted. Incorporating dynamic analysis with Sea State 8 and the survival current flowing from left to right in Fig. 1 produced maximum total anchor load (static + dynamic) of 9380 N on the left-hand anchor. This value was 10% larger than the weight in water of the anchor and slightly above the limit of the anchor's measured holding power. The decision to use additional 1000-lb DorMor anchors was based on this calculation and the possibility that such conditions could occur during a hurricane. The maximum total tension predicted in the simulation occurred just below the left-hand subsurface buoy and had a magnitude of 11 900 N. This was well below the breaking strength of the shackles (191 000 N) and sling links (160 000 N) that attach the vertical mooring line to the subsurface buoy. The maximum tension was also significantly below the breaking strength of the ½-in. chain (69 000 N) and ⅜-in. wire rope (62 000 N) that were the principal components of the mooring legs. The dynamic tensions in the vertical mooring legs, as measured by the standard deviation, were between 710 and 830 N. The highest dynamic loads of 1400 N occurred at the midpoint of the horizontal cable. All of these dynamic loads were small enough that the effects of cyclic fatigue could be ignored (Grosenbaugh 1995).

b. Design conditions

A uniform current parallel to the plane of the array depressed the upstream buoy and lifted the downstream buoy (Fig. 2). The horizontal cable became pitched at a small angle and shifted as a whole in the direction of the current. At the same time, the ends of the vertical

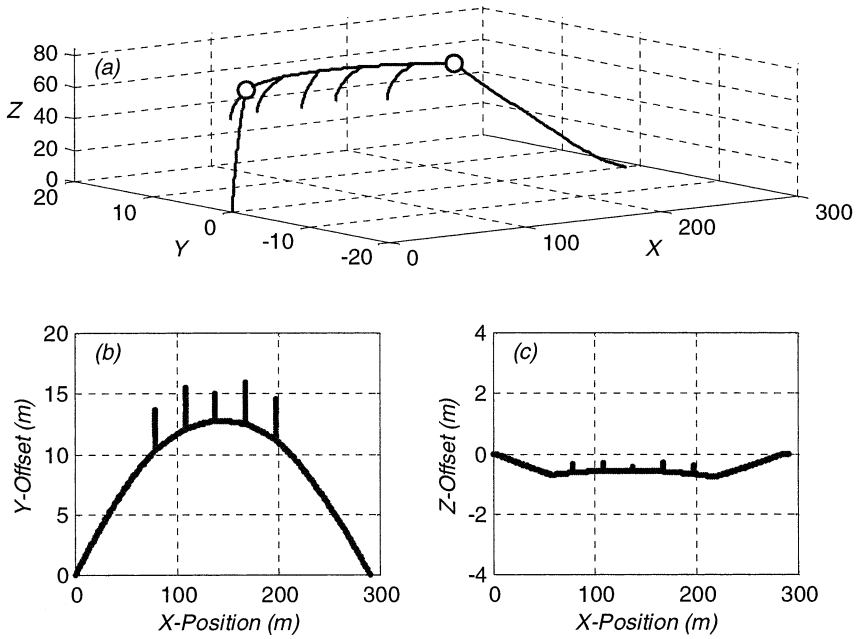

FIG. 3. Calculated static shape and offsets of mooring in a 0.5 m s^{-1} uniform current that is perpendicular to the array plane. (a) The three-dimensional deformation. (b) The out-of-plane horizontal offsets. (c) The vertical offsets of the anchor legs, horizontal cable, and temperature strings as a function of the original in-plane horizontal position.

instrument strings became displaced also in the direction of the current. For a uniform current of 0.5 m s^{-1}, the horizontal offsets (X offsets) along the horizontal cable were nearly constant and equal to 2.1 m. The vertical offsets along the horizontal cable ranged from -2.0 m at the upstream buoy to 2.3 m at the downstream buoy.

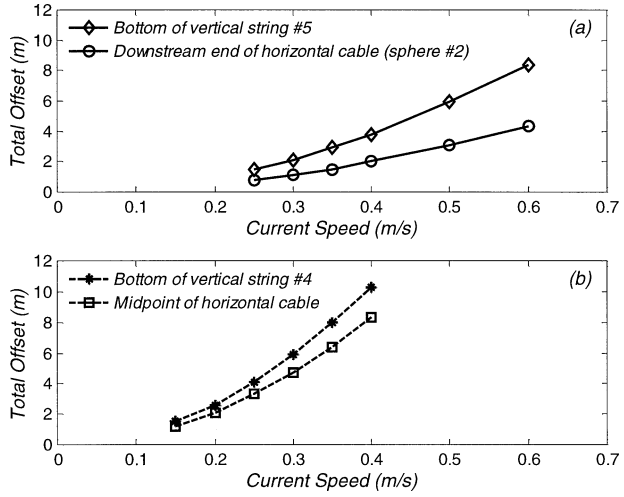

FIG. 4. Total offsets (combined vertical and horizontal) due to uniform currents. Offsets were measured at one location on the horizontal cable and at the bottom of one of the vertical instrument strings. (a) Current was parallel to the array plane: the offsets are given at the downstream end of the horizontal cable and at vertical string 5. (b) Current was perpendicular to the array plane: the offsets are given at the midpoint of the horizontal cable and at the bottom of vertical string 4.

The maximum horizontal offset of 5.5 m and the maximum total offset of 5.9 m occurred at the bottom of the downstream vertical instrument string. This offset was large because it represented a combination of the shift of the horizontal cable to which the vertical instrument string was attached and the response of the vertical instrument string itself to the current. For a uniform current perpendicular to the plane of the array (Fig. 3), the whole array was pushed over in the direction of the current with almost all the offset due to the out-of-plane horizontal shift (Y offsets). Again, the tops of the vertical instrument strings were displaced with the horizontal cable, and the bottoms of the strings were displaced further in response to the currents. For a 0.5 m s^{-1} current, the maximum horizontal offset of 15.9 m, which occurred at the bottom of vertical string 4, demonstrates the lack of stiffness of the mooring to currents in this direction. Most of the offset was due to the geometric changes incurred by the horizontal cable. The middle instrument string (vertical string 3) was not displaced as much because it had a different and heavier suite of attached sensors.

Figure 4 shows the static performance of the horizontal mooring in response to different uniform current speeds. The top panel shows the response to currents parallel to the direction of the mooring (0° inclination angle) and flowing from left to right in Fig. 1. For this current direction, the maximum total offsets occurred at the downstream end of the array (see Fig. 2). For this reason, the total offsets (combined vertical and horizontal) are given in Fig. 4a for the downstream end of

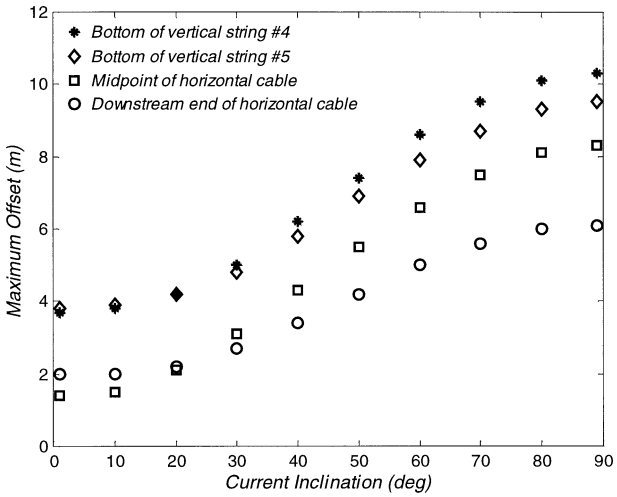

FIG. 5. Total offsets at four locations (same locations as in Fig. 4) on the array as a function of current inclination. The 0° inclination corresponds to a current that is parallel to the plane of the array. The 90° inclination corresponds to a current that is perpendicular to the plane of the array.

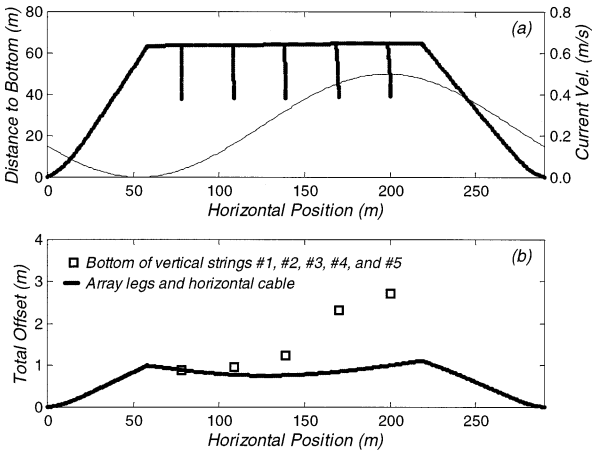

FIG. 6. Response of the horizontal mooring to a current that is periodic in the horizontal direction with a wavelength equal to 290 m and decreases linearly with depth. The peak current velocity at 20 m (the depth of the horizontal cable) is 0.5 m s^{-1}. The current decreases to zero at the sea bottom. (a) The static shape of the array (bold line) and the horizontal variation of the current at depth 20 m (fine line). (b) The total offsets of the anchor legs and horizontal cable (solid line) and the total offset of the bottom of the five vertical instrument strings (symbols).

the horizontal cable (sphere 2) and at the bottom of the downstream instrument string (vertical string 5). The bottom panel shows the results for a current that is perpendicular to the horizontal cable (90° inclination angle). The total offsets for this current direction are given for the midpoint of the horizontal cable and the bottom of vertical string 4, again because these are the locations of the maximum total offsets for this current direction (Fig. 3).

Next, consider the response of the array to a uniform current of 0.4 m s^{-1} as a function of current direction (Fig. 5). As the current direction rotates between 0° and 90°, the response (i.e., the total offsets) of the horizontal cable and the bottom of the vertical instrument strings follow a cosine response. The most dramatic increases occur for inclination angles greater than about 20° when out-of-plane offsets begin to dominate the total response. Berteaux and Walden (1981) suggested modifications to the planar design used in this study that would stiffen the response to out-of-plane currents, though for this experiment it was known that the strongest currents (from internal waves) were nearly unidirectional.

Based on the desired specifications for the total offsets to be less than 2.0 m for positions on the horizontal cable and less than 4.0 m for the bottom of the vertical instrument strings, we concluded that the horizontal mooring, as designed, could operate in uniform currents of up to 0.40 m s^{-1} directed at angles of up to 20°. Based on the results for the 90° case, the mooring could operate in uniform currents of up to 0.20 m s^{-1} from any direction (Fig. 4).

Under most circumstances, the current velocity will vary spatially both horizontally and vertically. In order to look at spatial variability of the current on the mooring configuration, we applied a current profile that varied sinusoidally in the horizontal direction and decreased linearly with depth. The current profile had maximum amplitude of 0.5 m s^{-1} at the nominal depth of the horizontal cable (water depth of 20 m) and a minimum value of 0.0 m s^{-1} at the bottom (water depth of 84 m). As we show in the next section, this current profile is similar (especially in the horizontal direction) to those that we measured during the passage of internal waves. Figure 6 shows results using a current profile with a horizontal wavelength of 290 m, which is the distance between the anchors. The top panel shows the configuration of the mooring when the peak of the horizontal profile was located at the downstream end of the horizontal cable. The bottom panel shows the total offsets of the mooring legs and horizontal cable (solid line) and the total offset at the bottom of the five vertical instrument strings (symbols). A spatially varying current lessens the total offsets so that, at this wavelength, all components of the array meet the specifications of total offset less than 2.0 m for the horizontal cable and less than 4.0 m for the bottom of the vertical instrument strings. As the maximum in the current profile travels from left to right across the array, the offset of the horizontal cable element remains nearly constant, while the offsets of the vertical instrument strings follow the horizontal variation of the current profile.

Figure 7 shows the effect of wavelength on the total offset of the horizontal array and bottom of the vertical instrument strings. The behavior for large wavelengths corresponds to a uniform current in the horizontal direction but with a linearly decreasing current with depth. For wavelengths between 100 and 400 m, the maximum

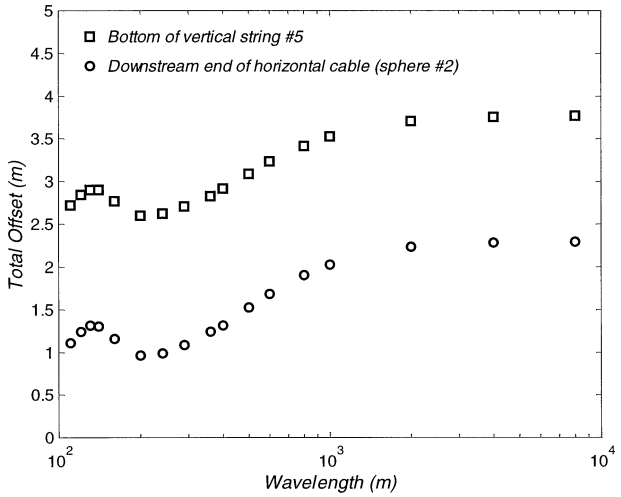

FIG. 7. Total offsets at the downstream end of the horizontal cable and at the bottom of the downstream vertical instrument string in the presence of the same current field used in Fig. 6 but as a function of the horizontal wavelength.

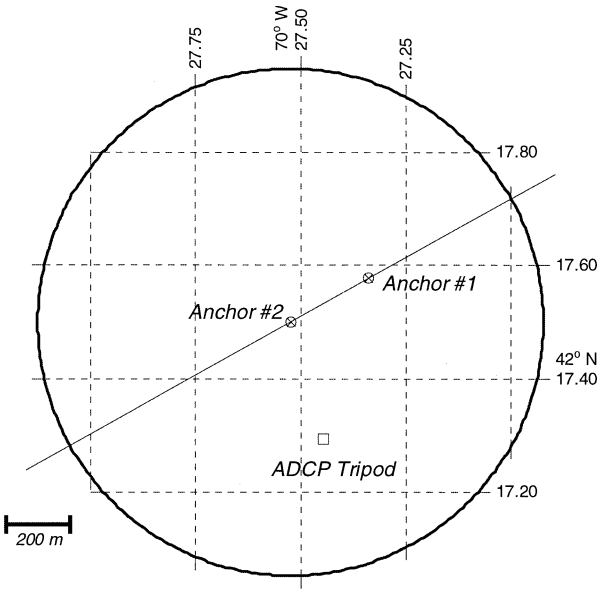

FIG. 8. Projection showing location of the horizontal mooring anchors and ADCP.

total offsets along the horizontal cable are less than 1.5 m. At the same time, the maximum offsets at the bottom of the vertical instrument strings are less than 3.0 m. As we show in the next section, the vertical current profiles corresponding to actual internal waves had strong flow reversals with depth that, in some cases, helped reduced maximum offsets of the bottom of the vertical instrument strings to less than 2.0 m.

Finally for the specified design conditions, the maximum dynamic motions along the horizontal cable did not occur at either subsurface buoy. The maximum motions were found, from simulations, to occur at the top and bottom of the upstream vertical instrument string. In the simulation, a uniform current of 0.5 m s^{-1} and Sea State 4 were applied to the mooring. The ranges of motions at the top of the upstream vertical instrument string were ± 0.24 m (horizontal motion) and ± 0.44 m (vertical motion). The motions at the bottom of the string were ± 0.08 m (horizontal motion) and ± 0.44 m (vertical motion). These values are within the specification of ± 0.5 m for dynamic motion. The small values are a direct result of placing the top of the array 20 m below the sea surface.

4. Mooring performance

The mooring was deployed from 6 August to 1 September 1998 in Massachusetts Bay near Stellwagen Basin at 42°17.5′N and 70°27.5′W (Fig. 8). The plane of the array was parallel to a line running 240° T. The line was perpendicular to the anticipated crests of the internal waves that travel from Stellwagen Bank toward the southwest across Stellwagen Basin during flood tides (Haury et al. 1979). The water depth at the deployment site was approximately 84 m. The nominal depth of the horizontal cable below the sea surface was approximately 20 m. The ends of the horizontal cable had a 1-m offset in zero current (Trask et al. 1999), possibly due to differences in the bottom depth. This was taken into account in the simulations. An upward-looking acoustic Doppler current profiler (RD Instruments 300-kHz Workhorse ADCP), which was deployed on a tripod 400 m south of the array, recorded the current velocity profile once every 60 s.

The ACMs and pressure sensors on the horizontal array were also self-recording and were sampled at a rate of 1 sample every 30 s. The internal time clocks of all the instruments including the ADCP were synchronized to Universal Time (± 1 s) just prior to the deployment. Drift of the internal clocks over the 27-day deployment was about 1–2 s. Thus, synchronization errors based on the sampling period of 30 s were at most 10%. Figure 9 shows the in-plane and out-of-plane current velocities sampled by the downstream acoustic current meter (ACM 3). Also shown are the vertical offsets of sphere 2 calculated from the pressure measurements. Positive spikes in the in-plane velocities and vertical offsets correspond to the passing of internal waves traveling approximately in the direction of 240° T. The magnitude of the out-of-plane velocity was always less than 0.25 m s^{-1} except for two instances when the propagation direction of the internal waves was skewed with respect to the plane of the array. In most cases, the in-plane velocity during the passage of internal waves was large enough that the overall current was directed within $\pm 20°$ of the plane of the array. The goal of the following analysis is to show how well the geometry of the array was maintained with the passing of these internal wave trains when they were traveling nearly parallel to the direction of the horizontal cable.

We chose the three internal wave events that had the

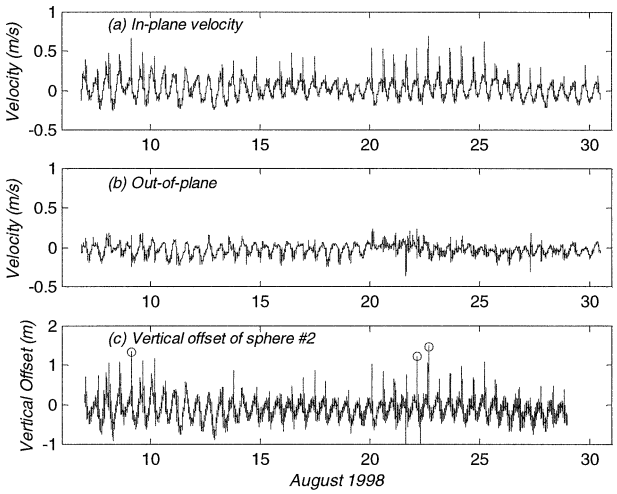

FIG. 9. Time records of (a) the in-plane current velocity and (b) out-of-plane current velocity measured by the ACM closest to sphere 2 (i.e., ACM 3). (c) The vertical offset of sphere 2 as measured by a pressure transducer. The three circles correspond to the three internal wave events that were used in the analysis of the field data.

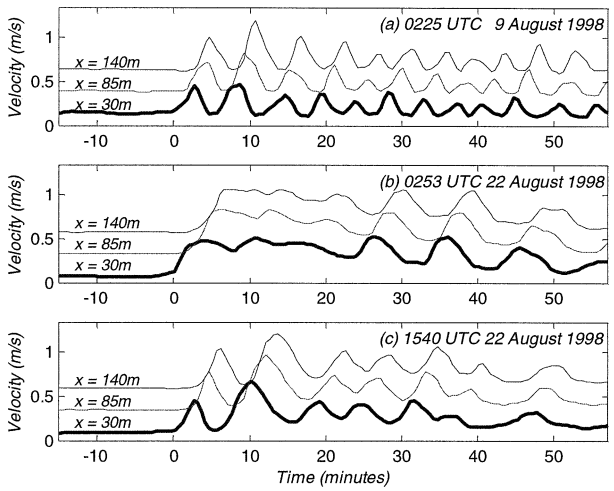

FIG. 10. Internal wave events for (a) 0225 UTC 9 Aug 1998, (b) 0253 UTC 22 Aug 1998, and (c) 1540 UTC 22 Aug 1998. Each panel shows the current velocity as recorded by the three ACMs that were spaced along the horizontal element at 30, 85, and 140 m from sphere 1. The velocities corresponding to the current meters at 85 and 140 m are displaced by 0.25 and 0.50 m s^{-1}, respectively, for clarity. The propagation direction of the internal waves for all three events was 240° T except for an 8-min period during the event depicted in (b) starting with the arrival of the first wave where the travel direction was 200° T.

highest currents and produced the largest vertical offsets (Fig. 9). The first of these events arrived at the upstream ACM (ACM 1) at 0225 UTC 9 August 1998 (Fig. 10a). This event exhibited a well-formed train of internal waves with a nearly constant propagation direction of 240°. This event had the second highest recorded current speed along the horizontal cable of the deployment, which was 0.68 m s^{-1} measured by the downstream ACM (ACM 3). The phase speed of the waves (based on cross correlation between ACM 1 and ACM 3) was approximately 0.69 m s^{-1}. The average period of the first three waves was about 360 s. The average period of the fourth, fifth, and sixth waves was reduced to about 270 s, and the period of the subsequent three waves was about 230 s. The corresponding wavelengths were 250, 180, and 160 m, respectively.

The second event that we chose for analysis arrived at 0253 UTC 22 August 1998 (Fig. 10b). The arrival was characterized by an initial plateau of about 0.5 m s^{-1} in the velocity record followed by a well-formed wave train. The maximum current velocity along the horizontal cable was 0.56 m s^{-1}. The maximum current speed of 0.59 m s^{-1} occurred 4 m below the horizontal cable. The propagation direction of the wave train was constant at 240° except for an 8-min period starting with the arrival of the first wave when the travel direction was 200°. The phase speed was approximately 0.56 m s^{-1}. The period was difficult to determine for the initial part of the record due to the fact that the internal waves were not distinct and the travel direction was not constant. However, the period corresponding to the three distinct internal waves that began arriving 25 min after the initial arrival was 570 s. This corresponds to a wavelength of 320 m.

The third event that we chose to analyze was the one with the strongest overall currents. It arrived at 1540 UTC 22 August 1998 (Fig. 10c). This event had a current speed of 0.70 m s^{-1} at the depth of the horizontal cable (20 m below the surface), but it had much stronger currents below that depth (up to 0.88 m s^{-1} at a depth of 34 m below the surface). The phase speed was approximately 0.56 m s^{-1}, which is the same value measured for the preceding event. The period appeared to decrease from 490 s (corresponding to the arrivals of the first two peaks) to 370 s (corresponding to the arrivals of the next three peaks). The wavelength, in this case, decreased from 270 to 210 m.

The analysis of each event involved calculating the time-varying shape of the horizontal array due to the time-varying current profile field. Because of the slowly varying nature of the current field, we used a quasi-static approach and assumed that inertial effects were negligible. At each instant in time, we estimated a velocity field in the plane of the array and used the static cable equations to determine the array shape. The time records of the three ACMs along with the phase speed of the internal waves were used to synthesize the horizontal current profile along the array at the depth of the horizontal cable. The horizontal profiles were constructed using a weighted average of the three ACMs and the assumption that the current field associated with the internal wave was constant in a reference frame that propagated at the wave speed. The weightings used in the averaging process depended linearly on the horizontal distance of the specified point from the ACMs. Figure 11 shows an example, from the 0225 UTC 9

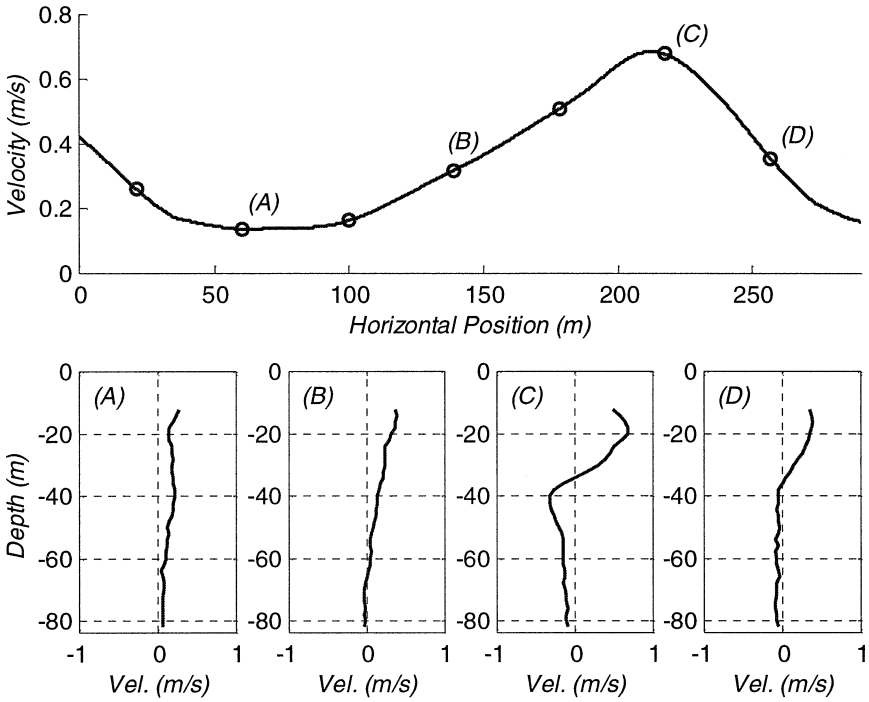

FIG. 11. Horizontal and vertical current profiles constructed from the ACMs mounted on the horizontal cable and the ADCP deployed nearby. The profiles represent a snapshot of the internal wave event shown in Fig. 10a at $t \approx 24$ min. (top) The horizontal current profile constructed from the ACMs and corresponding to a depth of 20 m, which is the nominal depth of the horizontal cable. The circles represent locations where there is a measured vertical current profile by the ADCP. (bottom) Four of the vertical profiles. The vertical profiles in the bottom panels correspond the lettered circles on the horizontal profile.

August 1998 event, of the horizontal profile that corresponded to the case when the peak of the second internal wave was located at the horizontal position of the downstream subsurface buoy (sphere 2). The vertical profile was determined from the ADCP data, which closely matched the ACM data at a depth of 20 m (even though there was some spatial averaging in ADCP data due to the spreading of the acoustic beams). The vertical profiles corresponding to a number of discrete phases of the traveling wave train were identified and normalized so that the vertical profiles from the ADCP data and the horizontal profiles constructed from the ACM data were consistent at a depth of 20 m. This process altered the values of the ADCP data by less than 5%. Examples of four of the vertical current profiles are given in Fig. 11. For each horizontal profile across the array, we would typically have about seven to nine vertical profiles spaced about 33 to 41 m apart. Interpolation between the vertical profiles was used to fill in the rest of the current field. For each event, we used 46 separate current fields spaced 1-min apart to reconstruct the time-varying motion of the array.

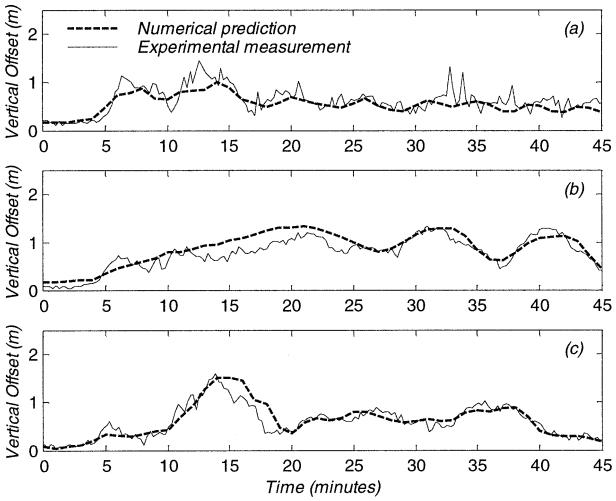

FIG. 12. Simulated and measured vertical offsets of the downstream subsurface buoy (sphere 2) as a function of time for the three internal wave events shown in Fig. 10.

The simulated results calculated by applying the interpolated current fields to the horizontal array for all three events are shown in Figs. 12 and 13 along with the actual measurements. Figure 12 compares the measured and simulated vertical offsets of the downstream subsurface buoy (sphere 2). Figure 13 compares the measured and simulated vertical offsets of the bottom of the downstream instrument string (vertical string 5). For all simulated results, the drag coefficient of the sub-

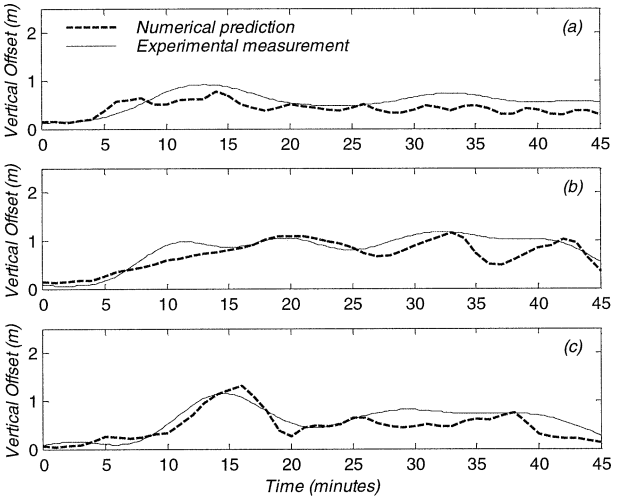

FIG. 13. Simulated and measured vertical offsets of the bottom of the downstream vertical instrument string (string 5) as a function of time for the three internal wave events shown in Fig. 10.

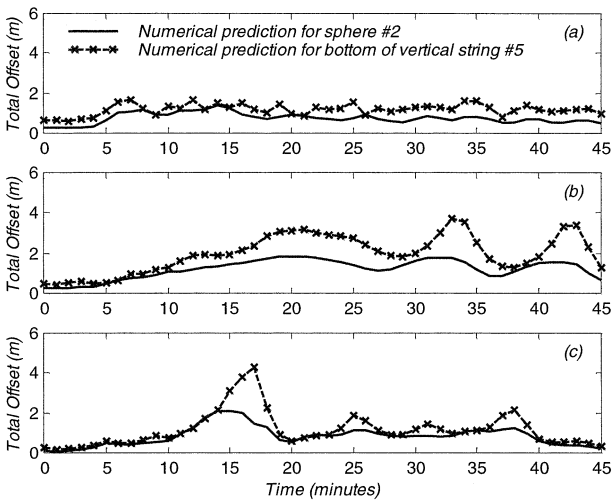

FIG. 14. Simulated total offsets (i.e., combined vertical and horizontal offsets) of the downstream subsurface buoy (sphere 2) and the bottom of the downstream vertical instrument string (string 5) as a function of time for the three internal wave events shown in Fig. 10.

surface buoys was 0.5, the drag coefficient of the attached instruments was 1.0, the drag coefficient of the wire rope was 2.0, and the drag coefficient of chain was 0.55 based on the outside chain-link width. These values are equal to the drag coefficients that we have used successfully in the past to simulate the response of single-point surface and subsurface moorings (Gobat and Grosenbaugh 1998). We did vary the sphere drag coefficient from 0.4 to 0.8 and found only a 10%–20% variation in the results.

These choices of drag coefficients gave a good overall fit to the data, though they systematically underestimated the vertical offsets at the beginning of each internal wave event. The most likely explanation of the underestimation was errors in the construction of the current field. Another possible explanation was flow effects near the pressure sensor that would elevate values of the measurements. This could also be the source of the high-frequency signal at the end of the time record in Fig. 12. Increasing the drag coefficients of the various mooring components would not explain the systematic underestimation because all of the simulated values would increase. Other regions where the vertical offsets of sphere 2 were underestimated or overestimated can be explained by errors in the construction of the current field or temporal variation of the drag coefficients. Differences between the measured and simulated vertical offsets of the bottom of vertical string 5 (Fig. 13) were slightly greater, and there appears to be more variation in the simulated response. This may be due to the characteristics of the low-pass filter built into the Brancker pressure sensor, which apparently filtered out much of the higher-frequency response.

The consistency of fit of the 138 separate simulations (46 for each of the three internal wave events) indicates that we can use the numerical model to analyze total offsets (which include the horizontal offsets) of the array elements. Figure 14 shows the total offsets of sphere 2 and the bottom of vertical string 5 that are associated with the vertical offsets presented in Figs. 12 and 13. The most noticeable features of this graph are the large total offsets that occur in Figs. 14b and 14c. For the bottom panel, the total offset of sphere 2 is predicted to be 2.1 m and the total offset of vertical string 5 is predicted to be 4.3 m (this is the only instance where the limits for total offset of the horizontal cable and the vertical instrument strings were exceeded in the simulations). In contrast, the total offsets in Fig. 14a were all less than 2.0 m. The reason for the difference is the variations in the vertical current profiles. Figure 15 shows currents profiles from the ADCP, for the three internal wave events (one profile per event). Each current profile corresponds to when the total offset of sphere 2 was at the maximum for that particular internal wave event. For the event at 0225 UTC 9 August 1998 (Fig. 14a), the maximum current was 0.68 m s^{-1} and occurred at the depth of the horizontal cable. There was a strong reversal in the current profile that created negative currents over the bottom half of the vertical instrument strings. For the two events on 22 August 1998, the reversal occurred below the bottom of the vertical instrument strings so that there were positive currents along their whole lengths. For the event at 0253 UTC 22 August 1998 (Fig. 14b), the maximum current was 0.59 m s^{-1}, and it occurred 4 m below the depth of the horizontal cable. For the event at 1540 UTC 22 August 1998 (Fig. 14c), a strong jetlike flow with maximum current velocity of 0.88 m s^{-1} developed about 14 m below the horizontal cable. Extending the vertical instrument strings to a greater depth would have actually reduced total offsets because they would have been sub-

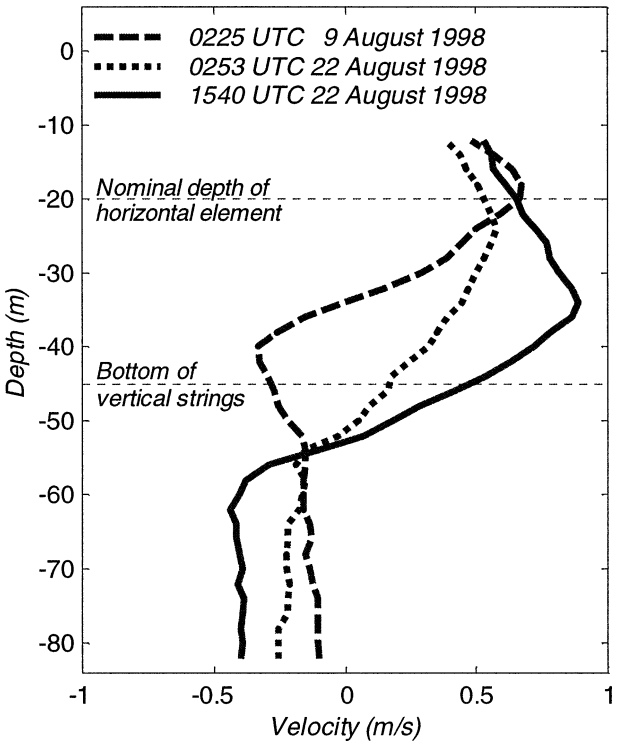

FIG. 15. Vertical current profiles corresponding to when the total offset of sphere 2 was a maximum for each of the three internal wave events.

jected to negative currents during the passage of the maximum current events. Even with total offsets of 2 m along the horizontal cable, errors in the measurement of the phase speed of the internal waves calculated from Fig. 10 are less than ±2%.

Wave-induced dynamic motion of the array was not a significant problem during the deployment. For most of the time, the significant wave height was less than 0.5 m. On 5 days out of the 27-day deployment, a Sea State 3 was achieved with significant wave heights of 1 to 1.5 m. For example, on 19 August 1998, the wind speed was almost 10 m s^{-1} from the north, the significant wave height was about 1.25 m, and the peak period was about 6.4 s (see 1998 historical records for National Data Buoy Center moored station 44013). To test the dynamic simulation capabilities of our numerical model, we used a modified Pierson–Moskovitz spectrum as input with the observed significant wave height and peak period and calculated the three-dimensional motion of sphere 2. This was compared to the response measured by the six-axis motion package mounted in the subsurface buoy (Fig. 16). The currents at this time, as measured by the ADCP, were nearly uniform with depth, had a magnitude of 0.11 m s^{-1}, and were flowing 115° T. Though, the shape of the actual wave train was different from that used as input to the simulation, the magnitude of the in-plane response (the measured significant peak-to-peak motion was 0.20 m vs simulated motion of 0.27 m) and out-of-plane response (the mea-

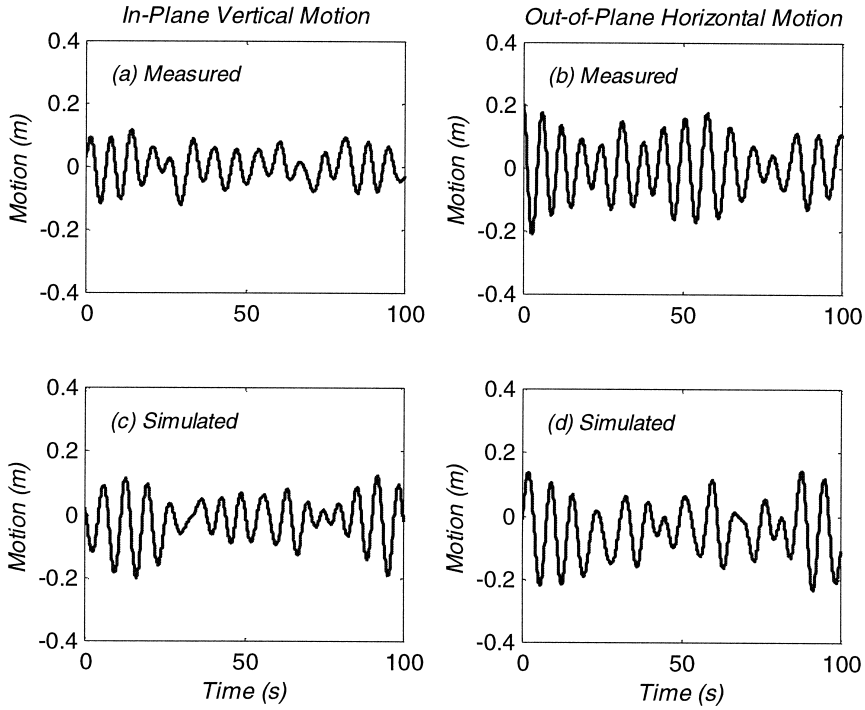

FIG. 16. Comparison between measured and simulated dynamic motion of sphere 2 in Sea State 3, which occurred on 19 Aug 1998. The sea state had a 1.25-m significant wave height and a 6.4-s peak period.

sured significant peak-to-peak motion was 0.37 m vs simulated motion of 0.34 m) compare well, further verifying the numerical code.

5. Conclusions

The most important result from our analysis is the comparison between the numerical simulations and the measured responses of the horizontal array to temporally and spatially varying currents and (to a lesser degree) random ocean waves. No previous study involving a two-dimensional cable array has had such a complete and complex set of current data, with timescales on the order of minutes and spatial scales on the order of the dimensions of the array itself. We have been able to use these data to construct time series of two-dimensional current fields that provide a demanding test for our numerical model. Using 45-min time series from three separate internal wave events, we have been able to show that a set of constant drag coefficients can provide an accurate fit to the measured vertical offsets at two locations on the horizontal array—at the downstream end of the horizontal cable and at the bottom of the downstream vertical instrument string. We argue that such a comparison provides verification of the numerical code and show its promise for performing future calculations on similar instrumented oceanographic arrays and aquaculture ''long-line'' moorings.

With regards to the specific performance of the horizontal array described in this paper, we have shown that the array can be used effectively on the continental shelf for measuring spatial variability in the upper mixed layer. The array can measure ocean phenomena in small to moderate currents and waves. We calculated that the array could maintain its geometry (within the specified limits) in uniform currents of up to 0.2 m s^{-1} from all directions and up to 0.4 m s^{-1} for uniform currents parallel to the plane of the array. Motion in Sea State 4 was predicted to be less than 1.0 m peak to peak. Adding spatial variability in the form of traveling periodic waves that were parallel to the plane of the array plane and that had a wavelength on the order of the array dimensions increased the operational envelope. The accuracy of the numerical model in calculating vertical offsets allowed us to confidently determine total offsets during the Massachusetts Bay internal wave experiment. Based on analysis of three of the strongest internal wave events, we concluded that the geometry of the main structure (horizontal cable and anchor legs) was kept to within ± 2.0 m of the nominal shape and the geometry of the vertical instrument strings was kept to within ± 4.0 m of the nominal shape even when the current velocity reached 0.70 m s^{-1}. These limits were exceeded for only one instance when the current velocity reached 0.88 m s^{-1}.

Acknowledgments. We would like to thank William Ostrom and Bryan Way of WHOI who played an integral part in the construction and deployment of the horizontal array. Funding for the development of the horizontal array was provided by the Office of Naval Research under Grant N00014-97-1-0158. Funding for the development of WHOI Cable was provided by the Office of Naval Research under Grant N00014-92-J-1269. Additional funding for the Massachusetts Bay internal wave experiment was provided by the U.S. Geological Survey.

REFERENCES

Anderson, S. P., and Coauthors, 1999: Measuring temperature and velocity variability from a horizontal mooring. *Proc. IEEE Sixth Working Conf. on Current Measurement,* San Diego, CA, IEEE, 139–143.

Berteaux, H. O., 1991: *Coastal and Oceanic Buoy Engineering.* Self-published, 285 pp.

——, and R. G. Walden, 1981: A feasibility study for a versatile deep sea, multileg, stable, cable array. Woods Hole Oceanographic Institution Tech. Rep. WHOI-81-13, 72 pp.

Blevins, R. D., 1990: *Flow-Induced Vibration.* Van Nostrand Reinhold, 451 pp.

Bonardelli, J. C., 1996: Long line shellfish culture in exposed and drift-ice environment. *Proc. Open Ocean Aquaculture Conf.,* Portland, ME, University of New Hampshire/University of Maine Sea Grant College Program, 235–252.

Geyer, W. R., G. B. Gardner, W. S. Brown, J. Irish, B. Butman, T. Loder, and R. Signell, 1992: Physical oceanographic investigation of Massachusetts and Cape Cod Bays. Massachusetts Bay Program Final Report, 497 pp.

Gobat, J. I., and M. A. Grosenbaugh, 1998: WHOI Cable: Time domain numerical simulation of moored and towed oceanographic systems. *Proc. Oceans '98,* Nice, France, IEEE, 699–705.

——, and ——, 2000: WHOI Cable v2.0: Time domain numerical simulation of moored and towed oceanographic systems. Woods Hole Oceanographic Institution Tech. Rep. WHOI-2000-08, 89 pp.

——, and ——, 2001: Application of the generalized-α method to the time integration of the cable dynamics equations. *Comput. Methods Appl. Mech. Eng.,* **190,** 4819–4827.

Goudey, C., and R. J. Smolovitz, 1996: Open-ocean culture of sea scallops off New England. *Proc. Open Ocean Aquaculture Conf.,* Portland, ME, University of New Hampshire/University of Maine Sea Grant College Program, 179–192.

Grosenbaugh, M. A., 1995: Designing oceanographic surface moorings to withstand fatigue. *J. Atmos. Oceanic Technol.,* **12,** 1101–1110.

Haury, L. R., M. G. Briscoe, and M. H. Orr, 1979: Tidally generated internal wave packets in Massachusetts Bay. *Nature,* **278,** 312–317.

Hoerner, S. F., 1965: *Fluid Dynamic Drag: Practical Information on Aerodynamic Drag and Hydrodynamic Resistance.* Hoerner Fluid Dynamics.

Kretshmer, T. R., G. A. Edgerton, S. A. Black, and N. D. Albertsen, 1975: An instrumented tri-moor for evaluating cable structure design methods. *Proc. Offshore Technol. Conf.,* **3,** 285–298.

Skop, R. A., and J. Mark, 1973: A Fortran IV program for computing the static deflections of structural cable arrays. Naval Research Laboratory Rep. NRL-FR-7640, 96 pp.

——, O. M. Griffin, and S. E. Ramberg, 1977: Strumming predictions for the SEACON II experimental mooring. *Proc. Offshore Technol. Conf.,* **3,** 61–66.

Thomson, N. W., 1996: Trends in Australasian open water shellfish culture. *Proc. Open Ocean Aquaculture Conf.,* Portland, ME, University of New Hampshire/University of Maine Sea Grant College Program, 223–234.

Trask, R. P., S. P. Anderson, B. S. Way, W. M. Ostrom, W. Paul, M. A. Grosenbaugh, J. I. Gobat, and R. W. Weller, 1999: The hor-

izontal mooring: A two-dimensional array, description of the array, components, instrumentation, deployment and recovery operations. Woods Hole Oceanographic Institution Tech. Rep. WHOI-99-14, 58 pp.

Weller, R. A., D. L. Rudnick, R. E. Payne, J. P. Dean, N. J. Pennington, and R. P. Trask, 1990: Measuring near surface meteorology over the ocean from an array of surface moorings in the subtropical convergence zone. *J. Atmos. Oceanic Technol.*, **7,** 85–103.

Williamson, C. H. K., and R. Govardhan, 1997: Dynamics and forcing of a tethered sphere in a fluid flow. *J. Fluids Struct.*, **11,** 293–305.